The Company of **Biologists**

RESEARCH REPORT

Local protein synthesis of neuronal MT1-MMP for agrin-induced presynaptic development

Jun Yu*, Marilyn Janice Oentaryo* and Chi Wai Lee‡

ABSTRACT

Upon the stimulation of extracellular cues, a significant number of proteins are synthesized distally along the axon. Although local protein synthesis is crucial for various stages throughout neuronal development, its involvement in presynaptic differentiation at developing neuromuscular junctions remains unknown. By using axon severing and microfluidic chamber assays, we first showed that treatment of a protein synthesis inhibitor, cycloheximide, inhibits agrin-induced presynaptic differentiation in cultured *Xenopus* spinal neurons. Newly synthesized proteins are prominently detected, as revealed by the staining of click-reactive cell-permeable puromycin analog O-propargyl-puromycin, at agrin bead-neurite contacts involving the mTOR/4E-BP1 pathway. Next, live-cell time-lapse imaging demonstrated the local capturing and immobilization of ribonucleoprotein granules upon agrin bead stimulation. Given that our recent study reported the roles of membrane-type 1 matrix metalloproteinase (MT1-MMP) in agrin-induced presynaptic differentiation, here we further showed that MT1-MMP mRNA is spatially enriched and locally translated at sites induced by agrin beads. Taken together, this study reveals an essential role for axonal MT1-MMP translation, on top of the well-recognized long-range transport of MT1-MMP proteins synthesized from neuronal cell bodies, in mediating agrin-induced presynaptic differentiation.

KEY WORDS: MT1-MMP, Local translation, Agrin, Presynaptic development, Neuromuscular junction

INTRODUCTION

It has been widely acknowledged that protein synthesis occurs not only in the neuronal cell bodies, but also distally in the dendrites and axons (Biever et al., 2019; Holt et al., 2019; Spaulding and Burgess, 2017). In the last decades, local protein synthesis has been reported in different stages of neuronal development, ranging from growth cone guidance to synaptic plasticity (Dalla Costa et al., 2021; Kim and Jung, 2015). Recent comprehensive axonal translatome analyses have indicated that compartment-specific mRNA translation supports the formation and maintenance of neural circuits *in vivo* (Shigeoka et al., 2016). However, whether local protein synthesis is required for presynaptic differentiation at developing neuromuscular junctions (NMJs) remains largely unclear.

School of Biomedical Sciences, Li Ka Shing Faculty of Medicine, The University of Hong Kong, Hong Kong.
*These authors contributed equally to this work

‡Author for correspondence (chiwai.lee@hku.hk)

M.J.O., 0000-0002-1798-3379; C.W.L., 0000-0003-4619-3189

At vertebrate NMJs, presynaptic differentiation involves the clustering of mitochondria and synaptic vesicles (SVs), two of the most prominent presynaptic markers (Lee and Peng, 2006). Nerve-derived agrin not only regulates postsynaptic differentiation in skeletal muscles (McMahan et al., 1992), but serves as a stop signal to mediate presynaptic differentiation in ciliary ganglion neurons (Campagna et al., 1995; 1997). Our recent study reported that focal agrin stimulation directs vesicular trafficking and surface insertion of membrane-type 1 matrix metalloproteinase (MT1-MMP, also named MMP-14), which functions to proteolytically remodel the extracellular matrix environment and cleave full-length low-density lipoprotein receptor-related protein 4 (LRP4) for agrin deposition and signaling during presynaptic differentiation in motor neurons (Oentaryo et al., 2020). Therefore, the temporally delayed expression of surface MT1-MMP is believed to serve as a molecular switch from axonal outgrowth to synaptogenic phase in mature neurons. Considering the inefficiency of transporting MT1-MMP proteins synthesized from the soma of highly polarized mature neurons, it is of interest to determine whether MT1-MMP can be locally translated at the presynaptic terminals.

Using axon severing and microfluidic chamber assays, this study first shows that local synthesis of axonal proteins is required for agrin-induced assembly of presynaptic specializations in cultured *Xenopus* spinal neurons through mammalian target of rapamycin (mTOR)/eukaryotic initiation factor 4E-binding protein 1 (4E-BP1) signaling pathway. Live-cell time-lapse imaging coupled with photobleaching/photoconversion experiments demonstrate that ribonucleoprotein (RNP)-containing granules are locally captured by agrin stimulation to regulate MT1-MMP mRNA localization and translation. Collectively, this study identifies a novel requirement of MT1-MMP local translation in mediating agrin-induced presynaptic development.

RESULTS AND DISCUSSION

Local protein synthesis is required for agrin-induced presynaptic development

To investigate the requirement of newly synthesized proteins in presynaptic differentiation, we first examined the effects of cycloheximide (CHX), a well-known protein synthesis inhibitor (Ennis and Lubin, 1964), on presynaptic differentiation in cultured *Xenopus* spinal neurons. Our recent study reported that agrin-coated beads induce structural and functional synaptic specializations along the neurites in a spatiotemporally controllable manner (Oentaryo et al., 2020). By adding 25 µM CHX to the cultured neurons before 4-h agrin bead stimulation, we found that agrin bead-induced mitochondrial and SV clustering were significantly inhibited (Fig. S1), indicating an essential requirement of newly synthesized proteins for the assembly of agrin-induced presynaptic specializations. Next, to determine whether the new proteins required for presynaptic differentiation are synthesized locally in axons, two parallel experimental approaches were adopted (Fig. 1A): (1) axons
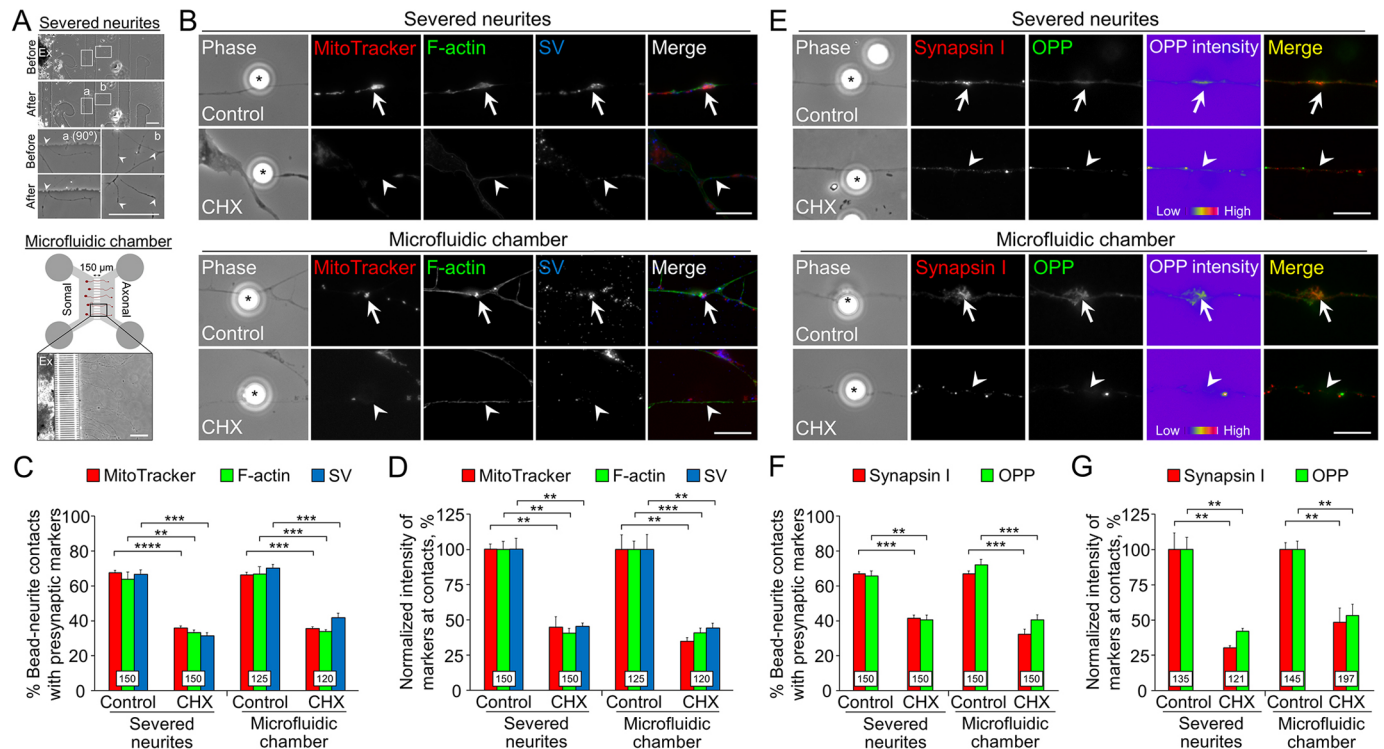
Fig. 1. Axonal protein synthesis is required for agrin-induced presynaptic development. (A) Experimental designs indicating the study of local protein synthesis in *Xenopus* neural explants (Ex) by neurite severing (top) or by using the microfluidic chamber (bottom). (B) Representative images showing the inhibition of agrin bead-induced presynaptic differentiation in the severed neurites by CHX treatment (top) or by treating the axonal compartment with CHX (bottom). (C,D) Quantitative analyses showing that CHX treatment significantly reduced the percentage of bead-neurite contacts with presynaptic markers (C) and their intensities (D) in either severed neurites or the microfluidic chamber. (E) Representative images showing the inhibition of agrin bead-induced synapsin I and OPP signals in the severed neurites by CHX treatment (top) or by treating the axonal compartment with CHX (bottom). Pseudocolor images (8-bit) highlight the relative fluorescence intensity of OPP signals. (F,G) Quantitative analyses showing CHX treatment significantly reduced the percentage of bead-neurite contacts with synapsin I and OPP signals (F) and their intensities (G) in either severed neurites or the microfluidic chambers. Asterisks indicate the bead-neurite contact sites. Arrows indicate the localization of presynaptic markers or OPP signals, whereas arrowheads indicate the absence of these markers, at the bead-neurite contacts. Data are mean±s.e.m.. Numbers indicated in the bar regions represent the total numbers of bead-neurite contacts measured from three independent experiments. **$P<0.01$, ***$P<0.001$, ****$P<0.0001$ (unpaired two-tailed Student's *t*-test). Scale bars: 100 µm (A); 10 µm (B,E).

were severed and separated from the somas mechanically; and (2) axonal compartments were separated from the somas physically using microfluidic chambers. Consistent with the data above, CHX treatment in severed neurites or in the axonal compartment of microfluidic chambers also significantly inhibited agrin-induced clustering of mitochondria and SVs, as well as the localization of actin cytoskeletal scaffolds (F-actin), at the bead-neurite contacts (Fig. 1B-D). To visualize newly synthesized proteins, we used O-propargyl-puromycin (OPP), a click-reactive cell-permeable puromycin analog that can be incorporated into the translating peptides (Kim and Jung, 2015). We found that OPP signals, together with a presynaptic phosphoprotein synapsin I, were spatially localized at agrin bead-neurite contacts in control groups but were significantly inhibited by CHX treatment in either severed axons or the axonal compartment of microfluidic chambers (Fig. 1E-G). Together, these results indicate that local protein synthesis is required for the assembly of agrin-induced presynaptic specializations. It is important to note that the motor neuron is the major neuronal type in *Xenopus* cultures, as postsynaptic acetylcholine receptor clustering is detected at up to 90% of contacts between spinal neurons and muscle cells (Peng et al., 2003). Intriguingly, agrin is also required for presynaptic differentiation in hippocampal neurons (Bose et al., 2000), but not in pontine explant cultures (Scheiffele et al., 2000), which suggests the possible cell-type specificity of agrin in the induction of presynaptic differentiation.

mTOR signaling regulates local protein synthesis for presynaptic development

We next investigated whether the well-studied mTOR signaling is involved in agrin-induced presynaptic development. Treatment with 0.2 µM rapamycin, an mTOR inhibitor (Tang et al., 2002), significantly inhibited agrin-induced formation of presynaptic specializations in either severed neurites or the axonal compartment of microfluidic chambers (Fig. 2A-C). Similar to CHX treatment, rapamycin treatment also effectively reduced the localized OPP and synapsin I signals at agrin bead-contacted sites (Fig. 2D-F).

Previous studies showed that mTOR promotes translation initiation through phosphorylating 4E-BP1 in cultured *Xenopus* neurons (Campbell and Holt, 2001; Piper et al., 2006). In our immunostaining experiments, p-mTOR and p-4E-BP1 signals were elevated at agrin bead-neurite contacts, whereas their total protein levels remained largely unchanged (Fig. 2G-H). However, rapamycin treatment in either severed neurites or the axonal compartment of microfluidic chambers greatly reduced p-mTOR and p-4E-BP1 signals at agrin bead-neurite contacts. As phosphorylated and total mTOR and 4E-BP1 proteins were probed by primary antibodies raised in the same species, we normalized each immunofluorescence marker intensity against a volume dye 5-(4,6-dichlorotriazinyl)-aminofluorescein (DTAF) (Schindelholz and Reber, 1999) to correct the differences in cell thickness. By
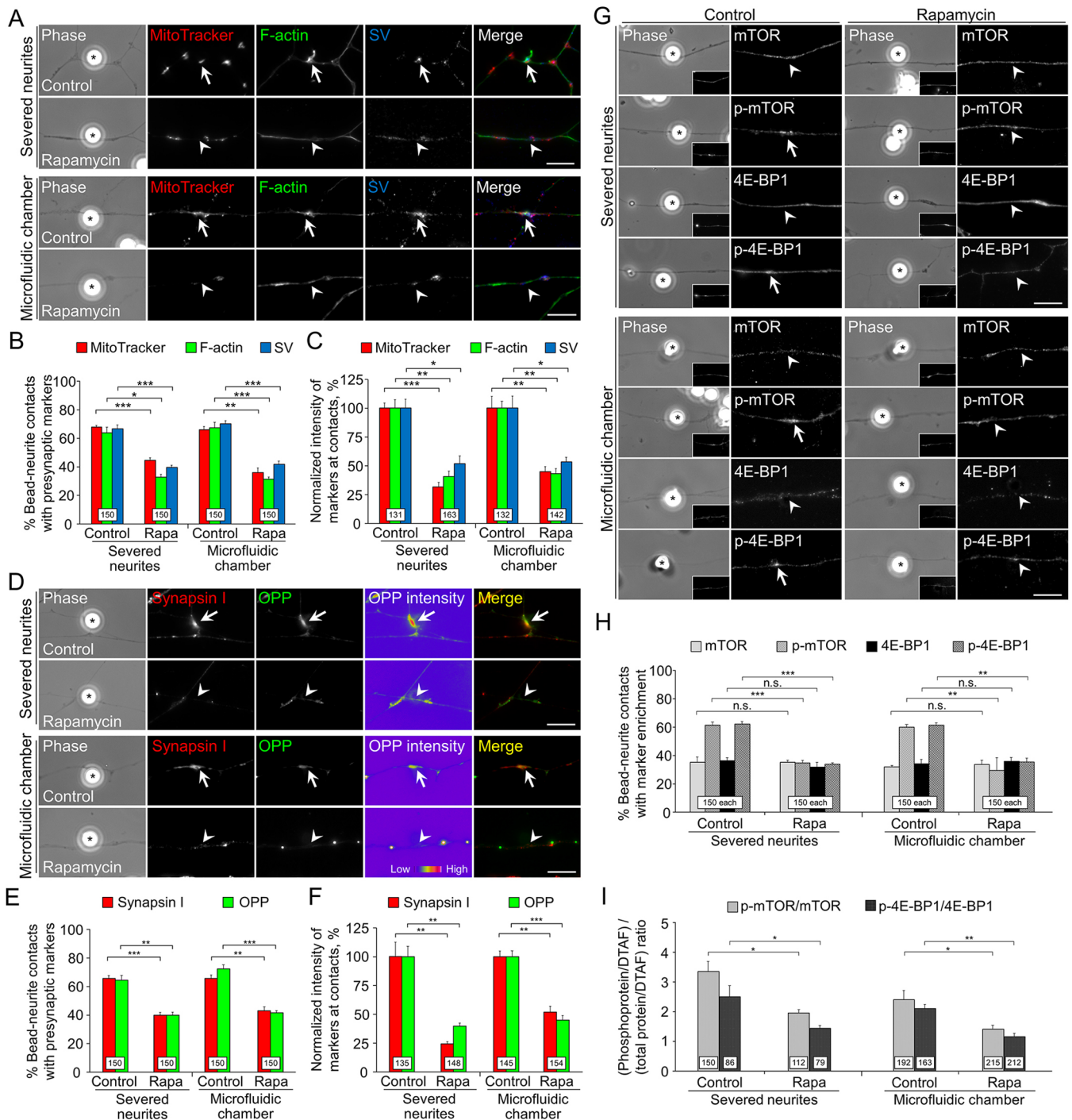
Fig. 2. Rapamycin inhibits agrin-induced mTOR and 4E-BP1 phosphorylation. (A) Representative images showing the inhibition of agrin bead-induced presynaptic differentiation in the severed neurites by rapamycin treatment (top) or by treating the axonal compartment with rapamycin (bottom). (B,C) Quantitative analyses showing that rapamycin (Rapa) significantly reduced the percentage of bead-neurite contacts with presynaptic markers (B) and their intensities (C) in either severed neurites or the microfluidic chambers. (D) Representative images showing the inhibition of agrin bead-induced synapsin I and OPP signals in the severed neurites by rapamycin treatment (top) or by treating the axonal compartment with rapamycin (bottom). Pseudocolor (8-bit) images highlight the relative fluorescence intensity of OPP signals. (E,F) Quantitative analyses showing that rapamycin significantly reduced the percentage of bead-neurite contacts with localized synapsin I and OPP signals (E) and their intensities (F) in either severed neurites or the microfluidic chambers. (G) Representative images showing the effects of rapamycin treatment in severed neurites (top panels) and in the axonal compartment of microfluidic chambers (bottom panels) on the phosphorylated (p-) versus total protein levels of mTOR and 4E-BP1 at agrin bead-contacted sites. Insets indicate DTAF fluorescence signals for normalization against the cell thickness. (H) Quantitative analyses showing the reduced percentage of bead-neurite contacts with localized signals of the phosphorylated, but not the total protein levels of, mTOR and 4E-BP1 by rapamycin treatment. (I) Quantitative analyses showing the reduced ratio of phosphorylated to total mTOR and 4E-BP1 intensities at agrin bead-contacted sites by rapamycin treatment. Fluorescence intensities were normalized against the DTAF signals. Asterisks indicate the bead-neurite contact sites. Arrows indicate the presence of localized signals, whereas arrowheads indicate the absence of localized signals, at the bead-neurite contacts. Data are mean±s.e.m.. Numbers indicated in the bar regions represent the total numbers of bead-neurite contacts measured from three independent experiments. *$P<0.05$; **$P<0.01$; ***$P<0.001$; n.s., not significant (unpaired two-tailed Student's t-test). Scale bars: 10 µm.

3

performing such indirect ratiometric analyses, we demonstrated that rapamycin significantly reduced the phosphorylation of mTOR and 4E-BP1 at the agrin bead-neurite contacts (Fig. 2I). These findings collectively demonstrate that agrin promotes local protein synthesis required for presynaptic differentiation through mTOR/4E-BP1 signaling.

Agrin induces local capturing and immobilization of RNP granules

The axonal trafficking of mRNA is mediated by RNA-binding proteins and transported in RNP granules (Korsak et al., 2016; Sahoo et al., 2018). To visualize and track RNP granule movement in live neurons, we expressed fluorescent uridine triphosphate (Cy3-UTP) in cultured spinal neurons. Kymograph analyses showed agrin beads induce a stable localization of Cy3-UTP-labeled RNP granules along the neurite (Fig. 3A, arrow). By contrast, the percentage of bead-neurite contacts with localized Cy3-UTP signals and their intensities were significantly reduced by adding the functional blocking anti-agrin antibody or by using the negative control bovine serum albumin (BSA) beads (Fig. 3A,B).

To further demonstrate local capturing of RNP granules by agrin beads, we next performed fluorescence recovery after photobleaching (FRAP) experiments. Before photobleaching, stable Cy3-UTP-labeled RNP granules were detected at two of the agrin bead-neurite contacts (Fig. 3C). Cy3-UTP fluorescence at one of the contacts was photobleached (dotted region), followed by time-lapse imaging to track the dynamic movement of Cy3-UTP signals into the photobleached region. In this example, a moving Cy3-UTP granule was found to be transported to, and subsequently immobilized at, the agrin bead-contacted site as early as 2.6 s after photobleaching (arrowheads). By examining seven bead-neurite contacts from three independent experiments, we observed local capturing of the first moving Cy3-UTP granule by agrin beads 11.88 ±5.33 (mean±s.d.) seconds after photobleaching. Kymograph analyses further indicated the local capturing of multiple Cy3-UTP granules in the photobleached region over time. By contrast, the localized Cy3-UTP-labeled RNP granules at another agrin bead-neurite contact outside the photobleaching region appeared to be very stable throughout the entire imaging period (white arrows). Intriguingly, we found that the majority of bead-neurite contacts (58.29%) exhibited both spatially localized Cy3-UTP signals and mitochondrial clusters 30 min after agrin bead stimulation and was greatly abolished by CHX treatment (Fig. S2), which is consistent with other studies showing the inhibition of stress-induced RNP granule formation by CHX (Kedersha et al., 2000; Panas et al., 2016). Therefore, our results indicate that agrin-induced Cy3-UTP localization and mitochondrial clustering are temporally coupled events with very little time delay. Nevertheless, it is still plausible that RNP granule localization may be detected preceding the clustering of presynaptic markers shortly after agrin stimulation. Given the implications of mRNA localization and RNA-binding proteins in NMJ development (Bélanger et al., 2003; Chang et al., 2012), our study provides evidence showing the capturing and immobilization of RNP granules for mRNA localization and translation during agrin-induced presynaptic formation and maintenance.

Agrin regulates MT1-MMP mRNA localization and translation

Our recent study suggested that the delayed temporal expression of surface MT1-MMP serves as a molecular switch from axonal outgrowth to the synaptogenic phase in neuronal development
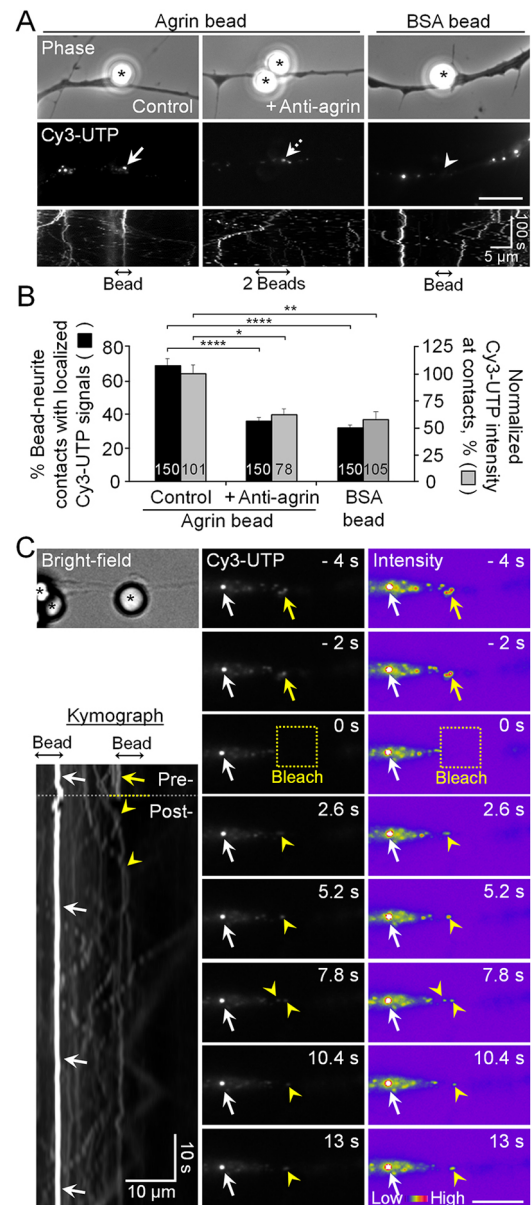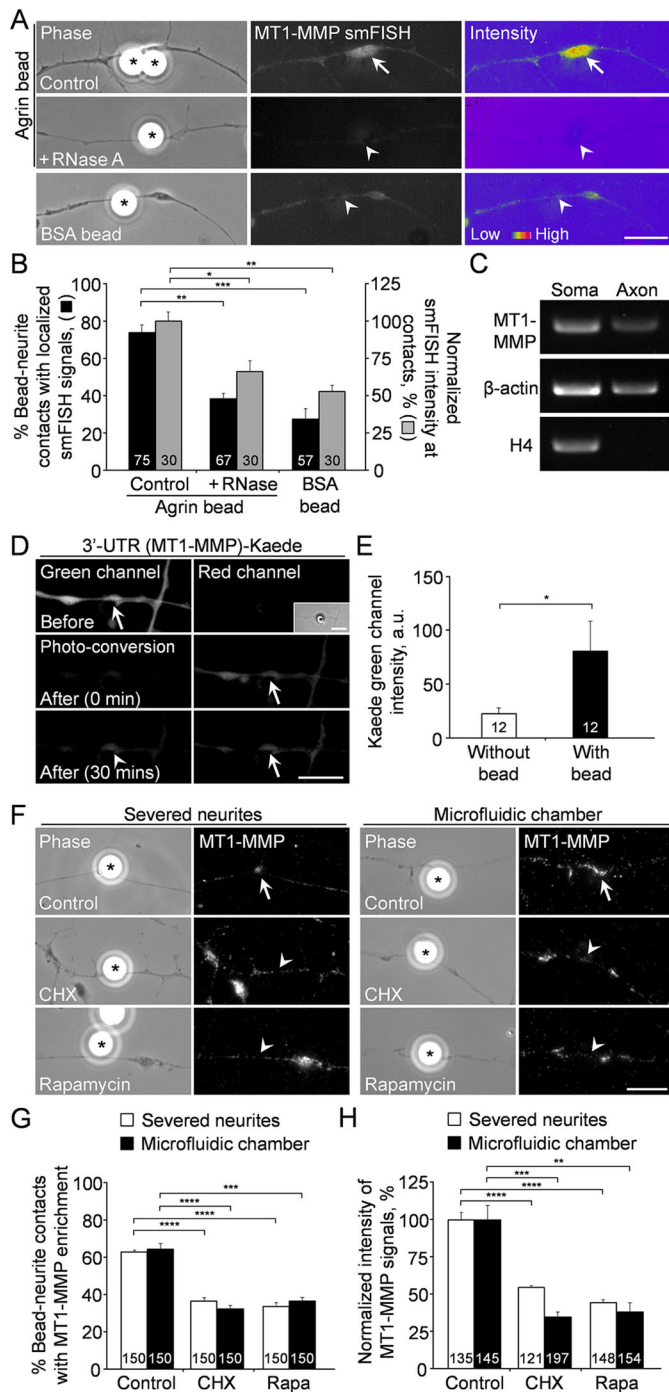

Fig. 3. Agrin induces local capturing and immobilization of RNP granules. (A) Representative images showing the dynamic transport of Cy3-UTP-labeled RNP granules and their immobilization at the agrin bead-contacted site (arrow). The dashed arrow indicates the transient Cy3-UTP localization at the bead contact in anti-agrin antibody-treated neurons. The arrowhead indicates the absence of Cy3-UTP signals contacted by the BSA bead. Kymographs (bottom panels) were constructed to show the stability of RNP granules. (B) Quantitative analyses showing the effects of anti-agrin antibody on the percentage of bead-neurite contacts with localized Cy3-UTP signals and their intensities. (C) A representative set of time-lapse images showing the local capturing of Cy3-UTP granules at agrin bead-neurite contact sites. Yellow arrows indicate localized Cy3-UTP signals at the bead-neurite contact before photobleaching (yellow dotted region). Arrowheads indicate the immobilization of moving Cy3-UTP granules at the bead-neurite contact sites over time. White arrows indicate the stability of Cy3-UTP-labeled RNP granules at another bead-neurite contact outside the photobleaching region. Pseudocolor (8-bit) images highlight the relative fluorescence intensity of Cy3-UTP signals. The kymograph shows agrin bead-induced immobilization of multiple Cy3-UTP-labeled RNP granules after photobleaching (arrowheads). Asterisks indicate bead-neurite contact sites. Data are mean±s.e.m. Numbers indicated in the bar regions represent the total numbers of bead-neurite contacts measured from three independent experiments. *P<0.05, **P<0.01, ****P<0.0001 (one-way ANOVA with Dunnett's multiple comparison test). Scale bars: 10 μm, unless specified otherwise.

Fig. 4. Agrin induces MT1-MMP local translation for presynaptic development. (A) Representative images showing the spatial enrichment of MT1-MMP mRNA molecules (arrows) at agrin bead-neurite contacts, which were largely reduced by RNase A treatment and not localized in BSA bead-neurite contacts (arrowheads). Pseudocolor (8-bit) images highlight the relative fluorescence intensity of MT1-MMP smFISH signals. (B) Quantitative analyses showing the reduced percentage of bead-neurite contacts with localized MT1-MMP smFISH signals and its intensities by RNase A treatment or BSA beads. (C) RT-PCR results showing the presence of MT1-MMP mRNA in both somal and axonal regions of cultured neurons. β-actin and H4 were used as positive and negative controls, respectively. (D) Representative images showing the axonal translation of photoconvertible Kaede proteins regulated by MT1-MMP 3′ UTR. Arrows indicate pre-existing Kaede proteins in severed neurites before and after photoconversion. Arrowhead indicates the newly synthesized Kaede proteins preferentially enriched at the site of agrin stimulation. Inset indicates the location of bead-neurite contact in the phase-contrast image. (E) Quantitative analysis showing the increased intensity of newly synthesized green Kaede proteins at agrin bead-contacted neurites 30 min after photoconversion. (F) Representative images showing the reduced spatial localization of MT1-MMP proteins at agrin bead-contacted sites by CHX or rapamycin treatment in severed neurites or in the axonal compartment of microfluidic chambers. Arrows indicate the spatially localized MT1-MMP signals, whereas arrowheads indicate the absence of MT-MMP localization, at the bead-neurite contacts. (G,H) Quantitative analyses showing that CHX or rapamycin treatment significantly reduced the percentage of bead-neurite contacts with localized MT1-MMP signals (G) and their intensities (H) in either severed neurites or microfluidic chambers. Asterisks indicate bead-neurite contact sites. Data are mean±s.e.m. Numbers indicated in the bar regions represent the total numbers of bead-neurite contacts measured from three independent experiments. *$P<0.05$, **$P<0.01$, ***$P<0.001$, ****$P<0.0001$ [one-way ANOVA with Dunnett's multiple comparison test (B,G,H) or paired two-tailed Student's t-test (E)]. Scale bars: 10 µm. a.u., arbitrary units.

compartments (Fig. 4C), like the well-known axonal translation target β-actin mRNA (Zhang et al., 2001). Our results are consistent with a recent study demonstrating that MT1-MMP mRNAs are present in mouse forebrain synaptosomal transcriptome (Merkurjev et al., 2018), further supporting the possibility of MT1-MMP local protein synthesis at presynaptic regions.

To visualize the sites of MT1-MMP mRNA translation, we generated a plasmid of the photoconvertible Kaede cDNA (Leung and Holt, 2008) linked with the 3′ untranslated region (UTR) of MT1-MMP. Upon 10-s UV photoconversion, all existing green Kaede proteins were photoconverted into red proteins in severed neurites, which ruled out the somal contribution of newly synthesized Kaede proteins afterwards. After 30 min, we detected newly synthesized green Kaede proteins preferentially localized at the agrin bead-neurite contact in severed neurites (Fig. 4D,E), indicating that agrin induces local translation of the linked reporter protein via MT1-MMP 3′ UTR. It is known that the 3′ and/or 5′ UTR sequences are involved in synaptic targeting of mRNAs along the axons (Holt et al., 2019). However, the exact mechanisms underlying the axonal transport and synaptic targeting of MT1-MMP mRNA warrant further investigation.

To further demonstrate the local translation of MT1-MMP mRNA at sites of agrin stimulation, we next performed immunostaining experiments that showed the spatial enrichment of endogenous MT1-MMP proteins at the agrin bead-neurite contacts in either severed neurites or the axonal compartment of microfluidic chambers, but this spatial localization was largely reduced after CHX or rapamycin treatment (Fig. 4F-H). As expected, MT1-MMP antisense morpholino oligonucleotide, which effectively suppresses endogenous MT1-MMP expression by interfering with its translation initiation (Chan et al., 2020a; Oentaryo et al., 2020), also reduced MT1-MMP localization at the bead-neurite contacts (Fig. S3).

(Oentaryo et al., 2020), indicating that MT1-MMP may be locally synthesized in axons of mature neurons. To test this, we performed single-molecule fluorescence *in situ* hybridization (smFISH) experiments that showed the spatial enrichment of MT1-MMP mRNA at agrin bead-neurite contacts (Fig. 4A,B). The specificity of MT1-MMP smFISH signals was validated by the treatment of RNase A and the addition of BSA beads, both of which largely abolished the localized signals at bead-neurite contact sites. Axonal RT-PCR analysis also revealed the presence of MT1-MMP mRNA in the pooled samples collected from both axonal and somal

In summary, compared with the well-documented MT1-MMP intracellular trafficking mechanisms in neurons and other cell types (Chan et al., 2020b; Poincloux et al., 2009), this study reveals a novel regulatory mechanism involving local MT1-MMP translation via the mTOR/4E-BP1 signaling pathway in presynaptic development. Although recent studies have provided compelling evidence demonstrating local protein synthesis in axonal branching and maintenance of *Xenopus* retinal ganglion cells *in vivo* (Wong et al., 2017; Yoon et al., 2012), technological advances in enhancing mRNA probe sensitivity and its specific targeting to the presynaptic motor neurons will be required in the future to allow us to further understand the regulation of MT1-MMP mRNA localization and translation at developing NMJs *in vivo*.

MATERIALS AND METHODS
DNA plasmids
To generate 3′ UTR (MT1-MMP)-Kaede reporter, Kaede (BamH1/EcoR1) was first amplified from pRSET-pr-Kaede (Addgene, 99228), and then subcloned into the empty pCS2+ plasmid using the following primers: forward, 5′-ACTGGTGGACAGCAAATGG-3′; and reverse, 5′-CTCGAATTCTTACTTGACGTTGTCC-3′. The 3′ UTR of *Xenopus* MT1-MMP was amplified with primers designed using the NCBI sequence (NM_001091009.1): forward, 5′-TAACCTCGAGATATGGAGCCTCT-GAGAGCA-3′; and reverse, 5′-TACGCTCGAGAAAAAACTGAATTTG-TTCATTTGAC-3′. The amplified fragment was then inserted into pCS2+ Kaede at the XhoI site.

Xenopus embryo microinjection and primary cell culture
The DNA construct encoding pCS2+3′ UTR (MT1-MMP)-Kaede was microinjected into the one-cell stage *Xenopus* embryos using an oocyte injector Nanoject (Drummond Scientific) as described previously (Lee et al., 2009, 2013). To visualize the localization of RNP granules, 13.8 nl Cy3-UTP (100 µM; ApexBio) was microinjected per embryo. To block the translation initiation of MT1-MMP mRNA, a custom-designed antisense morpholino oligonucleotide sequence against *Xenopus* MT1-MMP was used as reported previously (Oentaryo et al., 2020). Alexa Fluor 488-conjugated dextran (Thermo Fisher Scientific) was co-injected into the embryos as a fluorescent cell-lineage tracer.

Neural tubes were dissected from wild-type or microinjected embryos when they reached Nieuwkoop and Faber stage 19-22, and were then plated directly (for preparing neural explants) or treated with Ca^{2+}/Mg^{2+}-free solution before plating (for preparing dissociated neuron cultures) on acid-washed glass coverslips or microfluidic chambers coated with 71.4 µg/ml entactin-collagen IV-laminin (Merck Millipore). All experiments involving *Xenopus* frogs and embryos were carried out in accordance with the approved protocols of the Committee on the Use of Live Animals in Teaching and Research of The University of Hong Kong.

Cultured neurons were maintained in culture medium containing 10% Leibovitz's L-15 medium (v/v; Sigma-Aldrich), 87% Steinberg's solution [v/v; 60 mM NaCl, 0.67 mM KCl, 0.35 mM Ca(NO$_3$)$_2$, 0.83 mM MgSO$_4$ and 10 mM HEPES (pH 7.4)], 1% fetal bovine serum (v/v), 1% penicillin/streptomycin (v/v) and 1% gentamicin sulfate (v/v) at room temperature. To study local protein synthesis, the axons were severed by either removing the 1-day old explants or by separating the axonal from the somal compartments in microfluidic chambers. In experimental groups involving pharmacological treatment, CHX (ApexBio) or rapamycin (ApexBio) were added to the culture medium before neurite severing or 1 h before agrin bead stimulation. To locally induce presynaptic differentiation in cultured neurons or in severed neurites, 4.5 µm polystyrene beads (Polysciences) were coated with 100 µg/ml agrin (R&D Systems) according to the established protocol (Lee et al., 2009), or with 100 µg/ml BSA (Sigma-Aldrich) as the negative control. Notably, agrin or BSA beads were added into the neuronal cultures inside a laminar flow cabinet to avoid contamination. Before imaging experiments, the cultures were kept untouched for a minimum of 20 min to allow the beads to settle and make stable attachment with the neurites on the culture substrate. In most experiments, cells were fixed after 4-h bead stimulation, which has previously been demonstrated to induce the assembly of presynaptic specializations to the plateau level (Lee and Peng, 2006, 2008).

Live cell staining, cell fixation and immunostaining
To label mitochondria, coverslips or microfluidic chambers containing the live cultured neurons or severed neurites were stained with MitoTracker Red CMXRos (50 nM; Thermo Fisher Scientific) for 5 min. To detect the newly synthesized proteins, a Click-iT Plus OPP Alexa Fluor 488 protein synthesis assay kit (Thermo Fisher Scientific) was used according to the manufacturer's protocol. Coverslips or microfluidic chambers were fixed with 4% paraformaldehyde for 15 min, followed by cell permeabilization with 0.1% Triton X-100 for 10 min. After blocking in 2% BSA for 2 h in room temperature, cells were stained with the primary antibody for 2 h at room temperature or overnight at 4°C. Primary antibodies used in this study included anti-synaptotagmin (1:200; mAb48; Developmental Studies Hybridoma Bank), anti-synapsin I (1:1000; A6442; Thermo Fisher Scientific), anti-mTOR (1:50; 7C-10; Cell Signaling Technology), anti-p-mTOR (1:100; ab109268; Abcam), anti-4E-BP1 (1:100; 9644S; Cell Signaling Technology), anti-p-4E-BP1 (1:100; 9451S; Cell Signaling Technology) and anti-MT1-MMP (1:200; MAB3328; Millipore). It was followed by staining with Alexa Fluor secondary antibodies (1:400; Thermo Fisher Scientific) for 45 min. To normalize the thickness of neurites, cultures were stained with 2.5 µM DTAF (Sigma-Aldrich) for 20 min and then washed three times with PBS before mounting. Coverslips were mounted on glass slides with fluoromount-G mounting medium (Thermo Fisher Scientific).

Axonal RNA extraction and RT-PCR
In microfluidic chambers, 0.1 mg/ml recombinant agrin protein (R&D Systems) was added to the axonal compartment on day 2 for 24 h. After adding Trizol reagent (Invitrogen) to the axonal compartment, axonal materials were then collected. Axonal and somal materials from 160 chambers (neural tube tissues from five embryos per chamber) were pooled from four independent experiments, followed by RNA extraction using RNAiso Plus (Takara) according to the manufacturer's protocol. Total RNAs (750 ng) of each sample were reverse transcribed by using a high-capacity cDNA reverse transcription kit (Thermo Fisher Scientific). Somal (2 µl) and axonal (4 µl) cDNA samples were amplified by PCR of 40 cycles at 60°C annealing temperature using Phusion II High Fidelity DNA polymerase (Thermo Fisher Scientific) using a PCR thermal cycler (Takara). PCR primers for *Xenopus* MT1-MMP were designed based on the NCBI sequence (NM_001091009.1): forward, 5′-ATCTGCGGACACACA-CCTTA-3′; and reverse, 5′-GGCGTATCTCTTCCGTCTCA-3′. PCR primers for *Xenopus* β-actin and H4 were used as indicated in a previous study (Bellon et al., 2017): β-actin forward, 5′-CGTAAGGACCTCTATGCCAA-3′; β-actin reverse, 5′-TGCATTGATGACCATACAGTG-3′; H4 forward, 5′-GGCAAAGGAGGAAAAGGACT-3′, and H4 reverse, 5′-GAGAGCGTACACCACATCCA-3′.

smFISH
Cultured *Xenopus* spinal neurons were fixed in 4% paraformaldehyde in PBS for 10 min, followed by permeabilization in 70% ethanol overnight at 4°C. Sequences of 48 unique custom-designed Stellaris RNA FISH probes (Biosearch Technologies) against *Xenopus* MT1-MMP mRNA are listed in Table S1. Hybridization of Quasar 670 dye-labeled probes was carried out overnight in the dark at 37°C in accordance with the manufacturer's instructions. As a negative control, the cultures were subjected to RNase A treatment (200 µg/ml) before hybridization.

Photobleaching and photoconversion
In FRAP experiments, photobleaching was performed using an Axio TIRF unit fitted in a Nikon inverted microscope equipped with an oil immersion 100× NA 1.46 DIC objective lens. To obtain the baseline of fluorescence intensity before photobleaching, 11 images were taken at 0.2-s intervals on neurons expressing Cy3-UTP. Images were captured through Metamorph (Molecular Devices) using an Evolve 512 EMCCD camera (Photometrics).

The regions of bead-neurite contact sites in Cy3-UTP-expressing neurons were chosen for photobleaching. Photobleaching was performed by using an OBIS laser line (561 nm) with 80% laser intensity, which was kept the same for all FRAP experiments. After photobleaching, 150 images were taken at 1-s intervals to visualize the axonal movement of Cy3-UTP-labeled RNP granules. To quantify the FRAP experiments, the relative fluorescence intensity in the photobleached area was first measured and then normalized by the mean fluorescence intensity of the same region in the images acquired before photobleaching. Kymographs of fluorescence signals along the neurites were constructed from time-lapse series using ImageJ (National Institutes of Health).

For Kaede photoconversion experiments, explants were plated next to the microgrooves of microfluidic chambers. After being cultured for 2 days, neurites were severed to isolate the axons. Agrin beads were added in the axonal compartment of microfluidic chambers for 2 h. Photoconversion was performed by UV exposure on agrin bead-contacted severed neurites expressing Kaede signals for 10 s. The neurites were imaged at both green and red channels in 30 min after UV photoconversion.

Microscopy and data analyses

All other fluorescence imaging on live or fixed cells was acquired using an inverted wide-field fluorescence microscope (IX-83, Olympus), which was controlled via the imaging software Micro-Manager (Open Imaging). Images were taken using an ORCA-Flash 4.0 LT+ camera (Hamamatsu) with identical parameters between control and experimental groups. The percentage values were quantified by scoring 150 samples from three independent experiments, unless otherwise specified. For quantifying the fluorescence intensities, more than 50 samples from three independent experiments were collected and analyzed, unless otherwise specified. To quantify the normalized mean intensities of the presynaptic markers or OPP, the mean fluorescence signals at bead-neurite contacts were normalized with that at non-bead contact regions of the same neurites. In some experiments, immunostaining intensity of cytosolic protein markers was first normalized by DTAF signals to account for the difference in cell thickness. Data analyses were conducted using ImageJ, and the statistical analyses were performed using Prism 7 (GraphPad Software).

Competing interests
The authors declare no competing or financial interests.

Author contributions
Conceptualization: C.W.L.; Methodology: C.W.L.; Validation: J.Y., M.J.O., C.W.L.; Formal analysis: J.Y., M.J.O., C.W.L.; Investigation: J.Y., M.J.O., C.W.L.; Data curation: C.W.L.; Writing - original draft: J.Y., M.J.O., C.W.L.; Writing - review & editing: C.W.L.; Visualization: C.W.L.; Supervision: C.W.L.; Project administration: C.W.L.; Funding acquisition: C.W.L.

Peer review history
The peer review history is available online at https://journals.biologists.com/dev/article-lookup/doi/10.1242/dev.199000

References

Bélanger, G., Stocksley, M. A., Vandromme, M., Schaeffer, L., Furic, L., DesGroseillers, L. and Jasmin, B. J. (2003). Localization of the RNA-binding proteins Staufen1 and Staufen2 at the mammalian neuromuscular junction. J. Neurochem. 86, 669-677. doi:10.1046/j.1471-4159.2003.01883.x

Bellon, A., Iyer, A., Bridi, S., Lee, F. C. Y., Ovando-Vázquez, C., Corradi, E., Longhi, S., Roccuzzo, M., Strohbuecker, S., Naik, S. et al. (2017). miR-182 regulates Slit2-mediated axon guidance by modulating the local translation of a specific mRNA. Cell Rep 18, 1171-1186. doi:10.1016/j.celrep.2016.12.093

Biever, A., Donlin-Asp, P. G. and Schuman, E. M. (2019). Local translation in neuronal processes. Curr. Opin. Neurobiol. 57, 141-148. doi:10.1016/j.conb.2019.02.008

Bose, C. M., Qiu, D., Bergamaschi, A., Gravante, B., Bossi, M., Villa, A., Rupp, F. and Malgaroli, A. (2000). Agrin controls synaptic differentiation in hippocampal neurons. J. Neurosci. 20, 9086-9095. doi:10.1523/JNEUROSCI.20-24-09086.2000

Campagna, J. A., Ruegg, M. A. and Bixby, J. L. (1995). Agrin is a differentiation-inducing "stop signal" for motoneurons in vitro. Neuron 15, 1365-1374. doi:10.1016/0896-6273(95)90014-4

Campagna, J. A., Ruegg, M. A. and Bixby, J. L. (1997). Evidence that agrin directly influences presynaptic differentiation at neuromuscular junctions in vitro. Eur. J. Neurosci. 9, 2269-2283. doi:10.1111/j.1460-9568.1997.tb01645.x

Campbell, D. S. and Holt, C. E. (2001). Chemotropic responses of retinal growth cones mediated by rapid local protein synthesis and degradation. Neuron 32, 1013-1026. doi:10.1016/S0896-6273(01)00551-7

Chan, Z. C., Kwan, H. R., Wong, Y. S., Jiang, Z., Zhou, Z., Tam, K. W., Chan, Y. S., Chan, C. B. and Lee, C. W. (2020a). Site-directed MT1-MMP trafficking and surface insertion regulate AChR clustering and remodeling at developing NMJs. Elife 9, e54379. doi:10.7554/eLife.54379

Chan, Z. C., Oentaryo, M. J. and Lee, C. W. (2020b). MMP-mediated modulation of ECM environment during axonal growth and NMJ development. Neurosci. Lett. 724, 134822. doi:10.1016/j.neulet.2020.134822

Chang, Y.-F., Chou, H.-J., Yen, Y.-C., Chang, H.-W., Hong, Y.-R., Huang, H.-W. and Tseng, C.-N. (2012). Agrin induces association of Chrna1 mRNA and nicotinic acetylcholine receptor in C2C12 myotubes. FEBS Lett. 586, 3111-3116. doi:10.1016/j.febslet.2012.07.068

Dalla Costa, I., Buchanan, C. N., Zdradzinski, M. D., Sahoo, P. K., Smith, T. P., Thames, E., Kar, A. N. and Twiss, J. L. (2021). The functional organization of axonal mRNA transport and translation. Nat. Rev. Neurosci. 22, 77-91. doi:10.1038/s41583-020-00407-7

Ennis, H. L. and Lubin, M. (1964). Cycloheximide: aspects of inhibition of protein synthesis in mammalian cells. Science 146, 1474-1476. doi:10.1126/science.146.3650.1474

Holt, C. E., Martin, K. C. and Schuman, E. M. (2019). Local translation in neurons: visualization and function. Nat. Struct. Mol. Biol. 26, 557-566. doi:10.1038/s41594-019-0263-5

Kedersha, N., Cho, M. R., Li, W., Yacono, P. W., Chen, S., Gilks, N., Golan, D. E. and Anderson, P. (2000). Dynamic shuttling of TIA-1 accompanies the recruitment of mRNA to mammalian stress granules. J. Cell Biol. 151, 1257-1268. doi:10.1083/jcb.151.6.1257

Kim, E. and Jung, H. (2015). Local protein synthesis in neuronal axons: why and how we study. BMB Rep 48, 139-146. doi:10.5483/BMBRep.2015.48.3.010

Korsak, L. I., Mitchell, M. E., Shepard, K. A. and Akins, M. R. (2016). Regulation of neuronal gene expression by local axonal translation. Curr. Genet Med. Rep. 4, 16-25. doi:10.1007/s40142-016-0085-2

Lee, C. W. and Peng, H. B. (2006). Mitochondrial clustering at the vertebrate neuromuscular junction during presynaptic differentiation. J. Neurobiol. 66, 522-536. doi:10.1002/neu.20245

Lee, C. W. and Peng, H. B. (2008). The function of mitochondria in presynaptic development at the neuromuscular junction. Mol. Biol. Cell 19, 150-158. doi:10.1091/mbc.e07-05-0515

Lee, C. W., Han, J., Bamburg, J. R., Han, L., Lynn, R. and Zheng, J. Q. (2009). Regulation of acetylcholine receptor clustering by ADF/cofilin-directed vesicular trafficking. Nat. Neurosci. 12, 848-856. doi:10.1038/nn.2322

Lee, C. W., Vitriol, E. A., Shim, S., Wise, A. L., Velayutham, R. P. and Zheng, J. Q. (2013). Dynamic localization of G-actin during membrane protrusion in neuronal motility. Curr. Biol. 23, 1046-1056. doi:10.1016/j.cub.2013.04.057

Leung, K.-M. and Holt, C. E. (2008). Live visualization of protein synthesis in axonal growth cones by microinjection of photoconvertible Kaede into Xenopus embryos. Nat. Protoc. 3, 1318-1327. doi:10.1038/nprot.2008.113

McMahan, U. J., Horton, S. E., Werle, M. J., Honig, L. S., Kröger, S., Ruegg, M. A. and Escher, G. (1992). Agrin isoforms and their role in synaptogenesis. Curr. Opin. Cell Biol. 4, 869-874. doi:10.1016/0955-0674(92)90113-Q

Merkurjev, D., Hong, W.-T., Iida, K., Oomoto, I., Goldie, B. J., Yamaguti, H., Ohara, T., Kawaguchi, S.-y., Hirano, T., Martin, K. C. et al. (2018). Synaptic N(6)-methyladenosine (m(6)A) epitranscriptome reveals functional partitioning of localized transcripts. Nat. Neurosci. 21, 1004-1014. doi:10.1038/s41593-018-0173-6

Oentaryo, M. J., Tse, A. C.-K. and Lee, C. W. (2020). Neuronal MT1-MMP mediates ECM clearance and Lrp4 cleavage for agrin deposition and signaling in presynaptic development. J. Cell Sci. 133, jcs246710. doi:10.1242/jcs.246710

Panas, M. D., Ivanov, P. and Anderson, P. (2016). Mechanistic insights into mammalian stress granule dynamics. J. Cell Biol. 215, 313-323. doi:10.1083/jcb.201609081

Peng, H. B., Yang, J.-F., Dai, Z., Lee, C. W., Hung, H. W., Feng, Z. H. and Ko, C.-P. (2003). Differential effects of neurotrophins and schwann cell-derived signals on neuronal survival/growth and synaptogenesis. J. Neurosci. 23, 5050-5060. doi:10.1523/JNEUROSCI.23-12-05050.2003

DEVELOPMENT

Piper, M., Anderson, R., Dwivedy, A., Weinl, C., van Horck, F., Leung, K. M., Cogill, E. and Holt, C. (2006). Signaling mechanisms underlying Slit2-induced collapse of Xenopus retinal growth cones. *Neuron* **49**, 215-228. doi:10.1016/j.neuron.2005.12.008

Poincloux, R., Lizárraga, F. and Chavrier, P. (2009). Matrix invasion by tumour cells: a focus on MT1-MMP trafficking to invadopodia. *J. Cell Sci.* **122**, 3015-3024. doi:10.1242/jcs.034561

Scheiffele, P., Fan, J., Choih, J., Fetter, R. and Serafini, T. (2000). Neuroligin expressed in nonneuronal cells triggers presynaptic development in contacting axons. *Cell* **101**, 657-669. doi:10.1016/s0092-8674(00)80877-6

Sahoo, P. K., Smith, D. S., Perrone-Bizzozero, N. and Twiss, J. L. (2018). Axonal mRNA transport and translation at a glance. *J. Cell Sci.* **131**, jcs196808. doi:10.1242/jcs.196808

Schindelholz, B. and Reber, B. F. (1999). Quantitative estimation of F-actin in single growth cones. *Methods* **18**, 487-492. doi:10.1006/meth.1999.0817

Shigeoka, T., Jung, H., Jung, J., Turner-Bridger, B., Ohk, J., Lin, J. Q., Amieux, P. S. and Holt, C. E. (2016). Dynamic axonal translation in developing and mature visual circuits. *Cell* **166**, 181-192. doi:10.1016/j.cell.2016.05.029

Spaulding, E. L. and Burgess, R. W. (2017). Accumulating evidence for axonal translation in neuronal homeostasis. *Front. Neurosci.* **11**, 312. doi:10.3389/fnins.2017.00312

Tang, S. J., Reis, G., Kang, H., Gingras, A.-C., Sonenberg, N. and Schuman, E. M. (2002). A rapamycin-sensitive signaling pathway contributes to long-term synaptic plasticity in the hippocampus. *Proc. Natl. Acad. Sci. USA* **99**, 467-472. doi:10.1073/pnas.012605299

Wong, H. H.-W., Lin, J. Q., Ströhl, F., Roque, C. G., Cioni, J.-M., Cagnetta, R., Turner-Bridger, B., Laine, R. F., Harris, W. A., Kaminski, C. F. et al. (2017). RNA Docking and local translation regulate site-specific axon remodeling In Vivo. *Neuron* **95**, 852-868.e858. doi:10.1016/j.neuron.2017.07.016

Yoon, B. C., Jung, H., Dwivedy, A., O'Hare, C. M., Zivraj, K. H. and Holt, C. E. (2012). Local translation of extranuclear lamin B promotes axon maintenance. *Cell* **148**, 752-764. doi:10.1016/j.cell.2011.11.064

Zhang, H. L., Eom, T., Oleynikov, Y., Shenoy, S. M., Liebelt, D. A., Dictenberg, J. B., Singer, R. H. and Bassell, G. J. (2001). Neurotrophin-induced transport of a β-actin mRNP complex increases β-actin levels and stimulates growth cone motility. *Neuron* **31**, 261-275. doi:10.1016/S0896-6273(01)00357-9
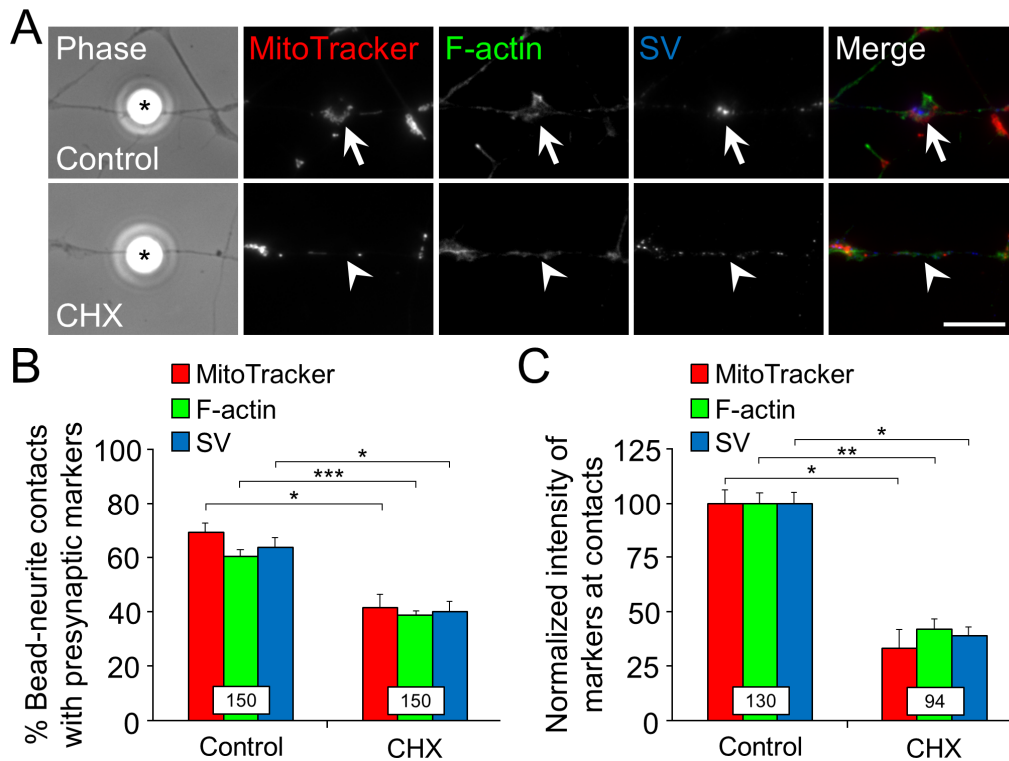
Figure S1. Agrin-induced assembly of presynaptic specializations requires newly synthesized proteins in cultured neurons.

(A) Representative images showing the inhibition of agrin bead-induced presynaptic differentiation in CHX-treated cultured neurons.

(B-C) Quantitative analyses showing the effects of CHX treatment on the percentage of agrin bead-neurite contacts with presynaptic markers (B) and their intensities (C).

Scale bar = 10 µm. Asterisks indicate the bead-neurite contact sites. Arrows indicate the localization of presynaptic markers, while arrowheads indicate the absence of these markers, at the bead-neurite contacts. Data are means ± S.E.M.. Numbers indicated in the bar regions represent the total numbers of bead-neurite contacts measured from 3 independent experiments. * $p < 0.05$, ** $p < 0.01$, and *** $p < 0.001$ (unpaired Student's t-test).
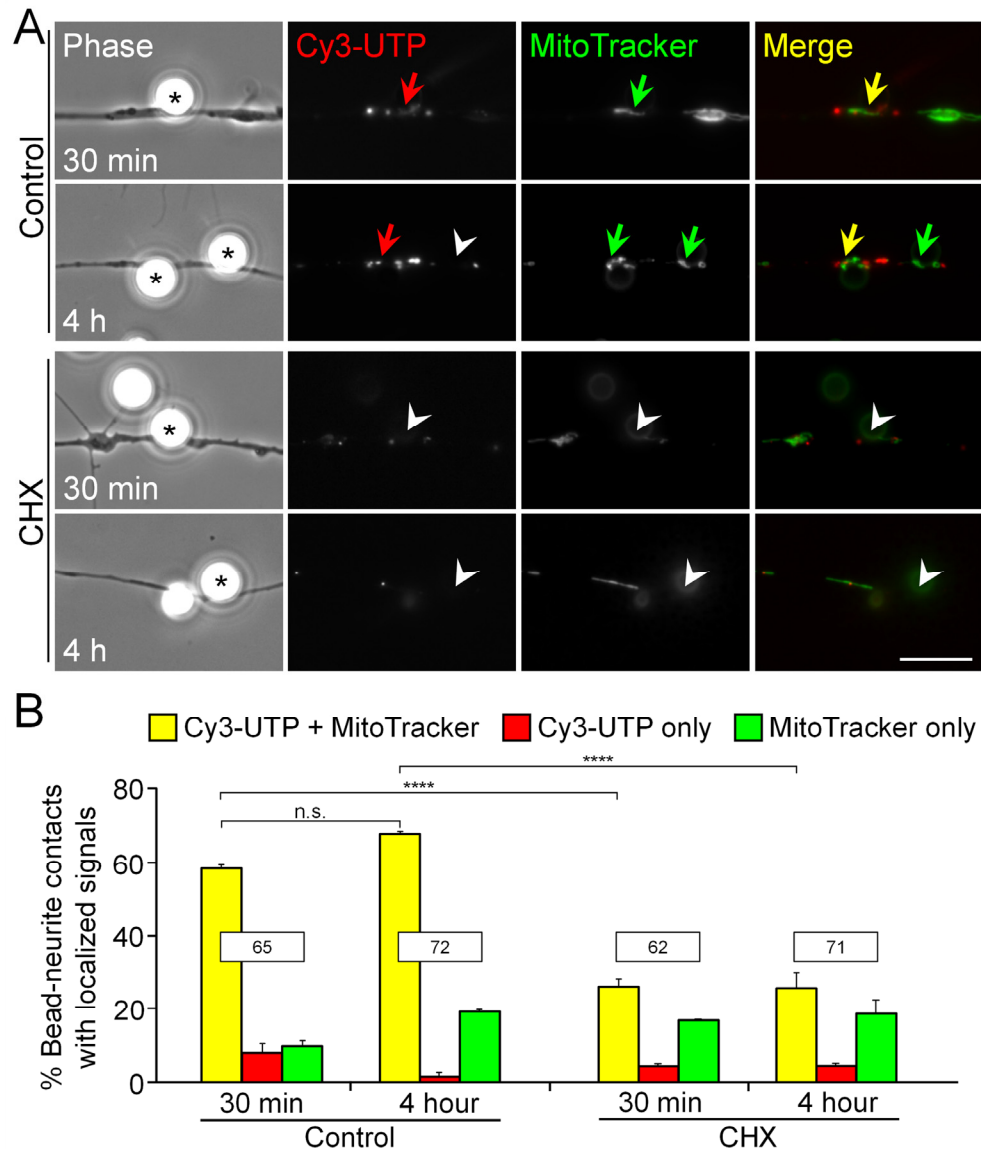
Figure S2. Agrin-induced Cy3-UTP localization and mitochondrial clustering are temporally coupled events via CHX-sensitive mechanisms.

(A) Representative images showing that both Cy3-UTP-labelled RNP granules and mitochondrial clusters were detected as early as 30-minute agrin bead stimulation, and they were significantly inhibited in CHX-treated neurons.

(B) Quantitative analyses showing the effects of CHX treatment on the localization of RNP granules and mitochondrial clusters induced by agrin beads for 30-minute or 4-hour.

Scale bar = 10 µm. Asterisks indicate the bead-neurite contact sites. Arrows indicate the localization of Cy3-UTP granules and mitochondrial clusters, while arrowheads indicate the absence of these markers, at the bead-neurite contacts. Data are means ± S.E.M.. Numbers indicated in the chart represent the total numbers of bead-neurite contacts measured from 3 independent experiments. n.s. = non-significant, **** p < 0.0001 (two-way ANOVA with Sidak's multiple comparison test).
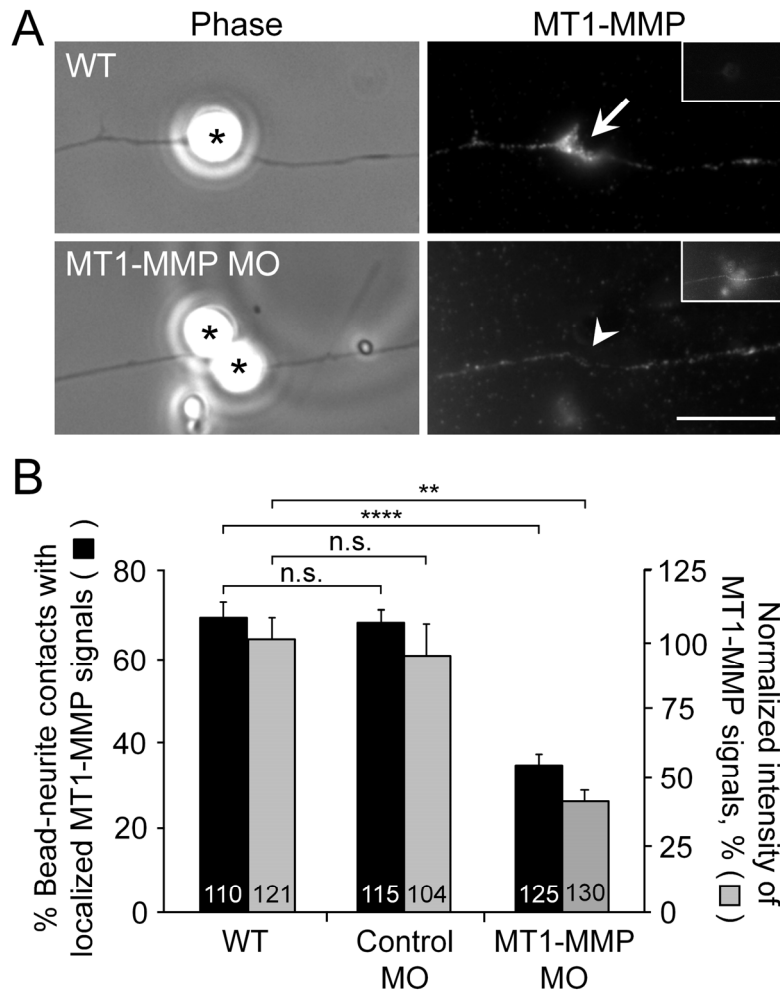
Figure S3. MT1-MMP antisense morpholino oligonucleotides inhibit agrin-induced localization of endogenous MT1-MMP proteins.

(A) Representative images showing the reduction of localized MT1-MMP immunostaining signals in MT1-MMP antisense morpholino oligonucleotide (MO)-expressing neurons, compared with that in wild-type (WT) or control MO-expressing neurons. Insets show the fluorescent dextran signals as a cell-lineage tracker.

(B) Quantitative analyses showing the reduced percentage of agrin bead-neurite contacts with localized endogenous MT1-MMP signals and their intensities in cultured neurons expressing MT1-MMP MO.

Scale bar = 10 µm. Asterisks indicate the bead-neurite contact sites. An arrow indicates the localization of endogenous MT1-MMP proteins, while an arrowhead indicates the absence of MT1-MMP localization, at the bead-neurite contacts. Data are means ± S.E.M.. Numbers indicated in the bar regions represent the total numbers of bead-neurite contacts measured from 3 independent experiments. n.s. = non-significant, ** $p < 0.01$, and **** $p < 0.0001$ (one-way ANOVA with Dunnett's multiple comparison test).

Probe ID	Sequence	Probe ID	Sequence
MT1-MMP_1	ccgagtatatttgctgtgac	MT1-MMP_25	gcaattgtgtcaaagttgcc
MT1-MMP_2	gttattcacagtgcatgcta	MT1-MMP_26	gaatacaaacatctctcccc
MT1-MMP_3	ttatccactgatctctgttc	MT1-MMP_27	tccatccattacacgtttat
MT1-MMP_4	ctgcagagcaagaatagggt	MT1-MMP_28	gaattgcccaataggcatag
MT1-MMP_5	atcctgtgcgactgagtaaa	MT1-MMP_29	ttaatggagctgggaagacc
MT1-MMP_6	aaacaggcaaatccaggctg	MT1-MMP_30	acaaatttgccatcctttcg
MT1-MMP_7	tctgggctgaatttggaagg	MT1-MMP_31	atcaaacacccagtgcttat
MT1-MMP_8	ggcagatatccatactgttg	MT1-MMP_32	gataccctggctctaaaaca
MT1-MMP_9	catagaacttctgcatggca	MT1-MMP_33	agcatcaattctgtcgctag
MT1-MMP_10	actgtcaaactttcctgtca	MT1-MMP_34	ttccatttggcatccaatat
MT1-MMP_11	cttcttcattgctttctctg	MT1-MMP_35	taatacttggtacccctgaa
MT1-MMP_12	caaatttgtcagggactcca	MT1-MMP_36	ctctcatctcctcgttaaac
MT1-MMP_13	aaatgtgatgtccttgtgct	MT1-MMP_37	ttgacaggtttggggtattc
MT1-MMP_14	cgcctcataggtagaatact	MT1-MMP_38	ctttgatggagtctgggatg
MT1-MMP_15	tcacactctcccaaacttta	MT1-MMP_39	gctgctgattgttgaacttc
MT1-MMP_16	gcatgatgtcagcatgttta	MT1-MMP_40	cgaccaaaacggatttcggg
MT1-MMP_17	ccatcaaaaggagtgctgtc	MT1-MMP_41	caggaactacaatggctgca
MT1-MMP_18	tatgcatgtgccaaaaagcc	MT1-MMP_42	ttgcctgaagagcacaacag
MT1-MMP_19	ggttctgcagagtcaaagtg	MT1-MMP_43	ccagtatagaatcctcttcg
MT1-MMP_20	ccaccaggaacagatcatta	MT1-MMP_44	agtgtaggtgttcacacttt
MT1-MMP_21	aatgttccaaaccgagagca	MT1-MMP_45	tggagaggcagtaattcagg
MT1-MMP_22	gagccataattgcagatgga	MT1-MMP_46	attgcattagcacttctctc
MT1-MMP_23	aattagttgtgtccatccac	MT1-MMP_47	ctggcagtgaaggggttaaa
MT1-MMP_24	ggatcatgtgggttatcatc	MT1-MMP_48	ttgagagaacaggccctaat

Table S1. A set of 48 unique sequences of Quasar 670-conjugated Stellaris RNA FISH probes against *Xenopus* MT1-MMP mRNA.